CORA Cork Open Research Archive
Cartlann Taighde Oscailte Chorcaí

Title	Heterogeneous Fenton-type oxidative degradation of low-density polyethylene to valuable acid products using a nanostructured Fe–CeO2 solid solution catalyst
Authors	Breen, Rachel;Holmes, Justin D.;Collins, Gillian
Publication date	2025-01-02
Original Citation	Breen, R., Holmes, J. D. and Collins, G. (2025) 'Heterogeneous Fenton-type oxidative degradation of low-density polyethylene to valuable acid products using a nanostructured Fe–CeO 2 solid solution catalyst', Catalysis Science & Technology, 15(3), pp.920-932. https://doi.org/10.1039/d4cy01384k
Type of publication	Article (peer-reviewed);journal-article
Link to publisher's version	10.1039/d4cy01384k
Rights	© 2025, Royal Society of Chemistry. All rights reserved.
Download date	2026-11-15 18:47:47
Item downloaded from	https://hdl.handle.net/10468/17403



UCC
University College Cork, Ireland
Coláiste na hOllscoile Corcaigh

Heterogeneous Fenton-type Oxidative Degradation of Low-Density Polyethylene to Valuable Acid Products Using a Nanostructured Fe-CeO_2 Solid Solution Catalyst

Rachel Breen[1,2], Justin Holmes[1,2], Gillian Collins[1,2]*

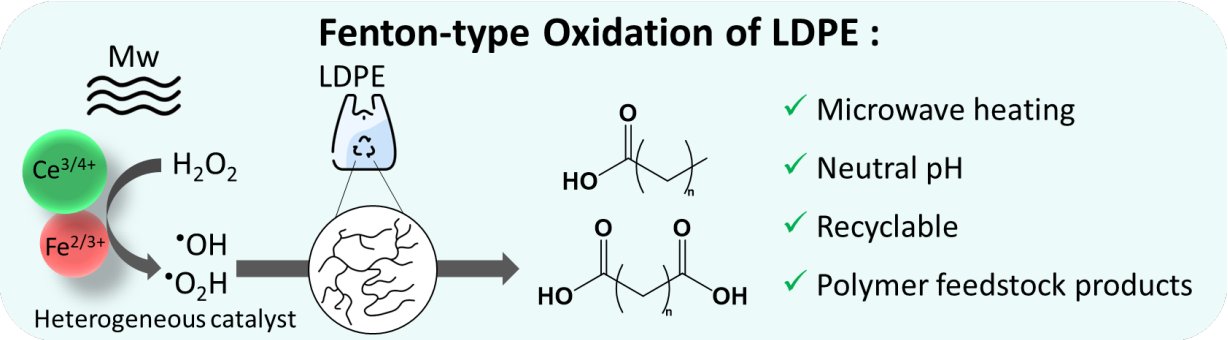
[1] School of Chemistry, University College Cork, Cork, T12 YN60, Ireland.

[2] AMBER Centre, Environmental Research Institute, University College Cork, Cork, T23 XE10, Ireland.

Abstract

The chemical conversion of waste plastic polymers to useful commodity chemicals has become crucial to helping tackle the issue of global plastic waste today. Polyolefins maintain the highest production rate and lowest recycling rate worldwide due to their inert chemical structures. This work shows the synthesis of solid-solution Fe-CeO_2 catalyst as an excellent heterogeneous catalyst for Fenton-type oxidative degradation of low-density polyethylene to achieve high yields of organic acids. The catalyst was synthesized in 3 molar ratios of Fe:Ce and it was found that the molar ratio of iron and cerium was crucial for catalytic performance with the Fe-CeO_2 1:1 catalyst giving the highest yields of acid products. The catalyst achieved 91 % mass loss and 71 % organic acid at pH 7, with 1 wt. % catalyst loading. The use of a multi-metal Fenton system resulted in a synergistic effect, displaying superior activity to systems with only one Fenton active metal. The heterogeneous nature of the catalyst this allowed for easy recovery and demonstrated excellent recyclability in multiple cycles. The high recyclability performance was attributed to the stability of the solid solution structure.

Keywords: heterogeneous catalysis, Fenton oxidation, solid solution catalyst, CeO_2, nanocatalysis, chemical recycling, oxidative degradation, low density polyethylene.



1. Introduction

Our over reliance on single-use plastics has become apparent by the ever-increasing production rates worldwide and uncontrollable accumulation of plastics in our environment. Today, we produce about 400 million tonnes of plastic waste annually with this figure projected to reach 1.1 billion tonnes in 2050.[1-3] A report in 2022 stated that only 9 % of plastic is recycled globally, while the rest is mismanaged (22 %), sent to landfill (49 %) or incinerated (19 %).[2] As a result of this, the use of chemical recycling to convert waste plastic into useful chemicals has gained huge traction in the world of research today. Many literature reports have shown methods of depolymerizing polymer plastics into useful monomers or commodity chemicals for use as feedstock in pharmaceutical, cosmetic or industrial fields.[4-7]

Chemical recycling of condensation polymers such as polyesters, polyamides and polycarbonates[8-10] to produce monomers and commodity chemicals has been widely researched. In contrast, chemical recycling of polyolefins such as low-density polyethylene (LDPE), linear low-density polyethylene (LLDPE) and high density polyethylene (HDPE) remain highly challenging due to the inert nature of their structures and the lack of polar functional groups along linear alkane chains.[11] LDPE has the highest primary waste generation out of all synthetic polymer plastics owing to its high production rate as a versatile polyolefin.[12] This high production rate is not met with equal recycling efforts, however, as only 3 % of recycled plastic worldwide is LDPE shown in Supplementary Information **Figure S1**. This is the lowest recycling rate of all other plastic polymers.[13] Alternative recycling efforts currently in place for polyolefins mainly involve high energy processes such as pyrolysis, gasification and hydrocracking.[14-16]

In more recent years, oxidative degradation processes have attracted growing interest as degradation pathways for polyolefins. The photocatalytic oxidation of polystyrene has been shown to produce aromatic oxygenates using graphitic carbon nitride[17] and $FeCl_3$[18]. In contrast, the more stable polyolefins such as PE require reactive or activated oxygen species to convert C-C polymers into small

oxygenated molecules.[19] Controlled thermolysis can produce longer chain fatty acids that can then be oxidized over manganese catalysts to produce valuable surfactants.[20] Microwave-assisted oxidative degradation of PE in nitric acid solutions yields dicarboxylic acid products, which are valuable for the production of polyesters and amides.[21, 22,] The use of nitric acid as a reaction media introduces undesirable side products such as NO_x gases and amine/amide degradation products.[21]

Fenton and Fenton-like advanced oxidation processes are well studied for environmental applications such as the destruction of a wide variety of organic pollutants, and contaminants[23, 24] Traditionally, Fenton's reagent involves the activation of H_2O_2 in the presence of Fe^{2+} and Fe^{3+} ions to produce hydroxy ($HO^{\bullet}$) and hydroperoxyl ($HO_2^{\bullet}$) radicals, which act as non-selective oxidants.[25] As the Fenton reaction takes place in aqueous medium without the need for hazardous or environmentally damaging organic solvents, it is a green and favourable oxidation process. Fenton oxidation can be a homogeneous (typically metal salts) or a heterogeneous process. Heterogeneous Fenton catalysts reported in the literature include iron oxides[26] and mixed metal oxides[27] as well as iron-based catalysts loaded on materials such as zeolites[28] and graphene oxide[29]. Heterogeneous Fenton-type catalysts have many benefits over homogeneous Fenton catalysts as they often can be used at a wider pH range, prevent iron sludge formation and can be more easily recovered which means they have the potential to be recycled.[30]

Fenton degradation has been reported in the literature for the oxidative degradation of microplastics (MP), where the aim is total destruction of the plastics to gaseous products rather than conversion to commodity chemicals.[31] Hu *et al.*[32] reported 96 % weight loss MPs in 16 h at a pH of ~1 using a homogeneous Fe^{2+} salt (4 mM) with 1 gL^{-1} MPs. Another group[33] reported reaction times of 7.5 h for MP degradation at a pH of 3 also using a homogeneous Fe^{3+} salt added at continual doses (5 doses of 750 mgL^{-1} 1 every 1.5 h) with 20 mgL^{-1} of MPs. Morŝar *et al.*[34] also reported the degradation of MPs using homogeneous Fe^{2+} at loadings of 10-12 wt. % with an optimal reaction pH of 3 but the reaction did not proceed in the absence of UV light for LDPE due to its structural stability, a common challenge encountered for LDPE.

Commonly, the efficiency of chemical plastic recycling is expressed in terms of the mass retention or diameter reduction, a measure that focuses only on whether the plastic waste is sufficiently degraded, rather than the products formed. [32, 34] The oxidation products are primarily short chain dicarboxylic acids which can be used as precursors to produce polymers and biopolymers and therefore depolymerisation protocols to maximize the yield of organic acids are hugely beneficial.

To overcome the inert nature of PE, a chemical pre-treatment with H_2SO_4 prior to Fenton degradation has been used to improve its hydrophilicity, followed by grafting of Fe^{3+} ions to the polymer. [35, 36] The

chemical pre-treatment enables milder reaction conditions and short reaction time but also results in the formation of undesirable sulfonated by-products. One interesting approach to overcome the chemical inertness of PE is mechano-catalytic oxidative cracking of PE to yield shorter alkane fragments as well as CO, CO_2, O_2, and H_2O as by-products, illustrating the diversity of the Fenton-type of chemistry for plastic degradation.[37] There is a gap in the literature for heterogeneous Fenton catalysts for LDPE degradation that require a low loading, no pretreatment, can be used at neutral pH, and can be tailored to produce useful acid products without over-oxidation to gaseous products.

While Fe is the traditional Fenton metal, the literature has been expanding to report many other redox active metals as excellent Fenton catalysts.[38] The incorporation of a second Fenton-active metal with Fe in mixed metal oxide systems has been widely reported to exhibit a strong synergistic effect.[39-42] CeO_2 is widely accepted as an excellent catalyst for many applications owing to its' ability to redox cycle between 3^+ and 4^+ states, resulting in high capacity for oxygen storage.[43, 44] These properties also make it an excellent Fenton catalyst, and it has been reported for use in organic pollutant degradation.[26] Commonly, CeO_2 is coupled with another metal typically by doping which results in the formation of oxygen vacancies, further improving catalytic activity.[45] Fe doped CeO_2 is a commonly reported catalyst for Fenton organic pollutant degradation[46, 47] owing to its stability, high surface area, reactivity, reusability and oxygen mobility.[48, 49] The dissolution of Fe in a larger crystal structure such as CeO_2 can create a superior Fenton-type catalyst as it can prevent precipitation and accumulation of soluble Fe sludge. Additionally, a synergistic effect is reported for iron/cerium complexes as Fenton catalysts.[47]

Microwave-assisted heating has proven to be beneficial for Fenton-type reactions by stimulating the redox cycle of metal ions. [50, 51] Microwaves can penetrate directly through a sample, forming hot spots on more polar or conductive species in a mixture.[52] In this case, Fe-doped ceria is an excellent microwave absorbing catalyst, meaning hot spots will be present on the catalyst surface improving reaction efficiency. Microwave assisted depolymerisation has also become popular for plastic degradation due to increased energy efficiency compared to conventional thermal heating.[53]

This work reports the synthesis of an Fe-CeO_2 solid solution as a catalyst for the microwave-assisted Fenton oxidative degradation of LDPE. The catalyst was characterised by XRD, Raman, XPS, FTIR, TXRF, SEM, TEM and EDX. The aim of this work is to maximise the yield of mono and dicarboxylic acids formed from LDPE oxidative degradation. Additionally, the catalyst was effective at low loadings (1 wt. %), at neutral pH and showed excellent recyclability over 6 cycles. To our knowledge, this is the first use of an Fe-CeO_2 solid solution recyclable heterogeneous catalyst for the Fenton oxidation of polyethylene under neutral pH.

Experimental Section

Experimental details including catalyst synthesis and characterisation, Fenton oxidation procedure and product analysis can be found in the Supplementary Information.

2. Results and Discussion

2.1 Synthesis & Characterisation of Fe-CeO_2 Catalyst

The Fe-CeO_2 solid solution catalysts were synthesized by co-precipitation method (see experimental section for details). **Figure 1** a) shows the Raman spectra collected for CeO_2, Fe_2O_3 and the Fe-CeO_2 composites made in 3 different molar ratios: 1:2, 1:1 and 2:1. The strong band arising at 468 cm^{-1} for the bare CeO_2 was assigned to the F_{2g} Raman mode of fluorite cubic ceria.[48, 54] Broadening of this band and a decrease in intensity was observed with increasing Fe content, indicative of Fe-Ce interaction in the doped systems. A notable shift of the fluorite peak to lower wavenumbers along with this decrease in intensity shows a decrease in the CeO_2 crystallite size likely due to the dissolution of Fe^{3+} ions throughout the CeO_2 lattice and formation of a solid solution. Broadening of the F_{2g} mode was also attributed to the presence of lattice defects.[55, 56] The modes at 227, 298, 404, 497 and 611 cm^{-1} were assigned to the A_{1g} or E_g modes of α-Fe_2O_3 and were only observed in the Fe_2O_3 and the Fe-CeO_2 2:1 catalyst due to saturation of the ceria lattice and formation of Fe_2O_3 on the catalyst surface. The absence of these peaks in the Fe-CeO_2 catalysts with a molar ratio of 1:2 and 1:1, is indicative of solid solution formation. The weaker intensity of the Fe_2O_3 Raman bands compared to those of CeO_2 were attributed to differences in crystallinity or particle size of the phases present[56], but have also been reported due to the strong absorbance of Fe_2O_3 in this region of the Raman spectrum.[55, 57]

The XRD patterns of the catalysts shown in **Figure 1** b) supports Raman analysis on formation of a solid solution. The diffraction peaks at 28.4, 32.9, 47.3, 56.2, 59.1, 69.3, 76.7 and 79.0° in 2θ were assigned to the (111), (200), (220), (311), (222) and (400) lattice planes of CeO_2 with a cubic fluorite ($Fm\bar{3}m$) crystal structure, respectively (JCPDS 65-5923). The presence of these peaks in the XRD pattern of each of the three solid solutions shows the preservation of the cubic fluorite CeO_2 structure on addition of the Fe^{3+}. Furthermore, the broadening and decreased intensity of the CeO_2 peaks in the solid solutions is commonly attributed to the shrinking of the overall lattice size on replacement of the larger Ce^{4+} ions with smaller Fe^{3+} ions. The iron oxide showed peaks at 21.1, 33.1, 36.5, 41.1, 50.3, 53.0, 58.9 and 61.2 ° in 2θ, are assigned to the (012), (104), (110), (113), (024), (116), and (018) lattice

planes of α-Fe_2O_3 (JCPDS 33-0664) in agreement with the literature.[58] These peaks are not observed in the Fe-CeO_2 catalysts with molar ratios of 1:1 and 1:2, consistent with the formation of a solid solution.[59] The CeO_2 crystallite size was also estimated using the Scherrer equation[60] in **Figure S2** (see Supplimentary Information) showing a decrease in size from 18 nm in the bare CeO_2 to 4.8 nm for the 1:2 catalyst, 2.9 nm for the 1:1 catalyst and 2.7 for the 2:1 catalyst. The decrease in crystallite size on addition of Fe to the CeO_2 lattice structure is to be expected as inclusion of smaller Fe ions into the CeO_2 lattice will shrink the overall lattice size. A small decrease in crystallite size was seen between the Fe-CeO_2 1:1 and Fe-CeO_2 2:1 catalysts due to the CeO_2 lattice becoming saturated with Fe ions and the crystallite size only slightly decreases as the excess iron is forming as Fe_2O_3 rather than being further incorporated into the CeO_2 lattice, as also observed in the Raman spectra and XRD patterns. FTIR analysis was also carried out on each of the catalysts shown in Supplementary Information **Figure S3**. The broad bands at 440 cm^{-1} and 525 cm^{-1} attributed to Fe-O stretching becomes less intense as the Fe content decreases in each of the solid solutions in excellent agreement with the Raman and XRD analysis. The broad band at ~3450 cm^{-1} was assigned to -OH stretching vibrations and is characteristic of adsorbed surface water molecules.[61]

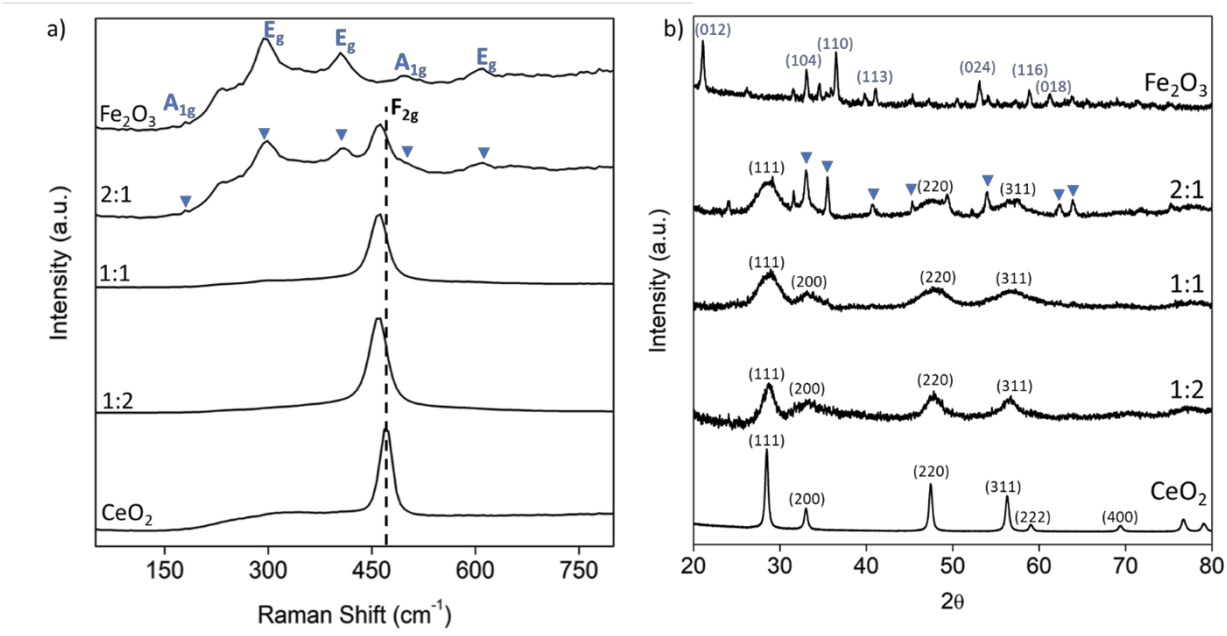


Figure 1: a) Raman analysis of Fe_2O_3, CeO_2, and Fe-CeO_2 solid solutions and b) XRD patterns of Fe_2O_3, CeO_2, and Fe-CeO_2 solid solutions.

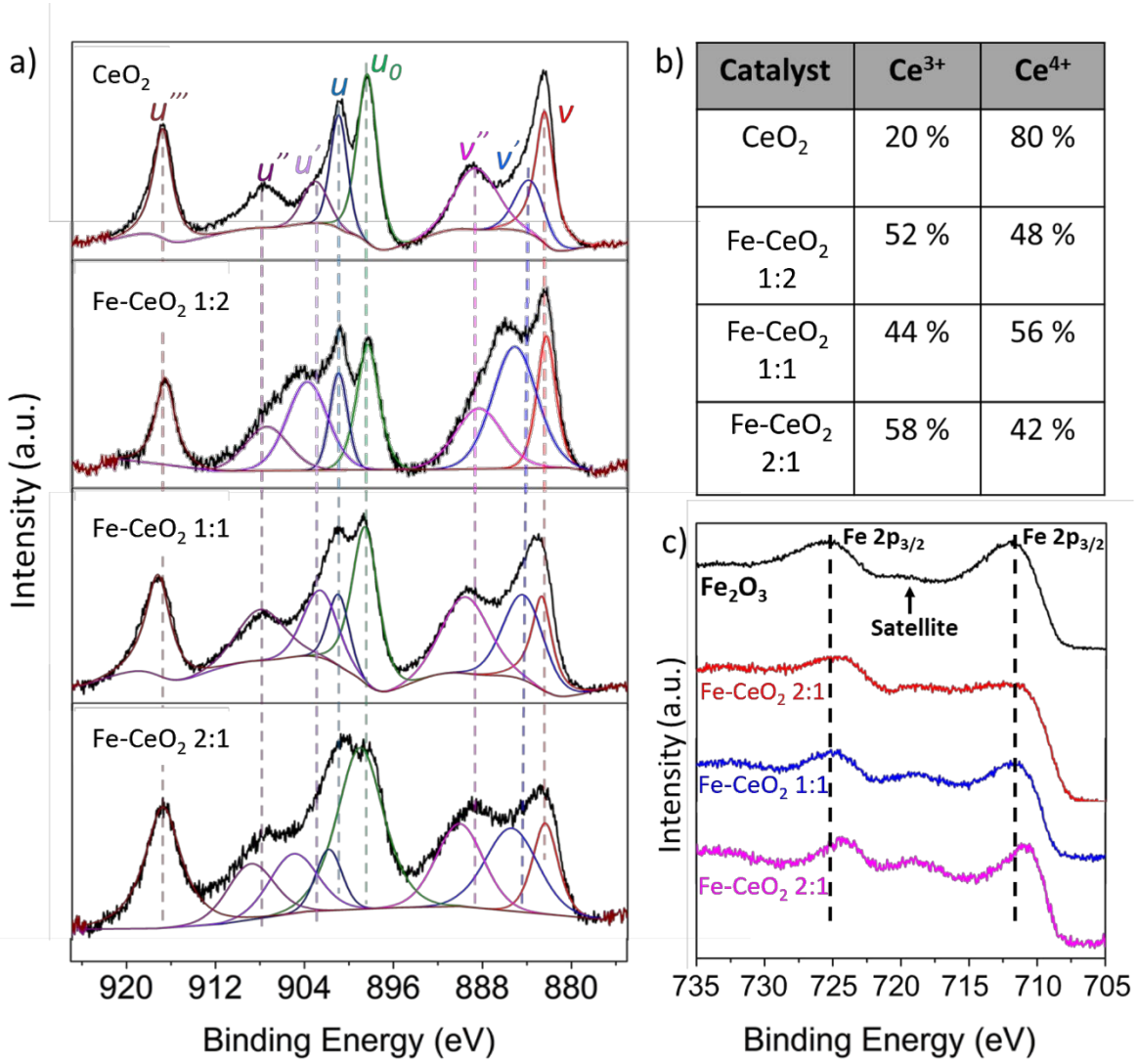
XPS analysis was used to assess the surface chemistry of the solid solutions, specifically the valence state of the cerium and iron species in the solid solution as well as the oxygen vacancies that were

present. XPS confirmed that Fe and Ce were present in ratios of 2:1, 1:1 and 1:2 for each respective catalyst and correlated well with other quantitative analysis on Fe and Ce carried out in this study. The survey scan for each catalyst is shown in Supplementary Information **Figure S4** and confirmed the presence of Fe and Ce within the samples. The Ce 3d region was used to establish the dominant oxidation state of Ce in each of the samples. The Ce 3d XPS spectra for bare CeO_2 and each of the solid solutions, shown in **Figure 2** a), were in excellent agreement with Ce 3d XPS spectra for CeO_2 in the literature[62, 63] and showed eight distinct peaks all corresponding to either Ce^{3+} or Ce^{4+} core levels. The peak labels *v* and *u* correspond to the spin-orbit doublets of Ce $3d_{5/2}$ and Ce $3d_{3/2}$, respectively. The quantitative data of Ce^{4+} and Ce^{3+} in CeO_2 and each of the solid solutions was calculated and is shown in **Figure 2** b). (see Experimental section for further details).

The peak denoted u''' is the reported fingerprint peak for Ce^{4+} Ce $3d_{3/2}$ state and was present in all samples.[64, 65] Additionally, the peaks denoted u, u'' and u''', and v, v'' and v''' are the final states of the Ce^{4+} Ce $3d_{3/2}$ and Ce $3d_{5/2}$, respectively. The final states for Ce^{3+} are expressed as u_0 and u', and v_0 and v', corresponding to the Ce $3d_{3/2}$ and Ce $3d_{5/2}$, respectively.[66] The percentage of Ce^{4+} sites dropped from 80 % in the CeO_2 sample to 48 %, 56 % and 42 % in the 1:2, 1:1 and 2:1 samples, respectively, and was attributed to the substitution of the Ce^{4+} sites with Fe^{3+} sites in the CeO_2 lattice on formation of a solid solution. An increase in Ce^{3+} sites from 20 % in CeO_2 to 52 %, 44 % and 58 % in the 1:2, 1:1 and 2:1 samples, respectively, and was associated with an increase in oxygen vacancies within the solid solution which have been shown to increase catalytic activity in CeO_2 systems.[61] Furthermore, the presence of Ce^{3+} and Ce^{4+} in an almost equal ratio in the catalyst will help to promote Fenton reactivity as discussed in the catalytic evaluation section.

Figure 2 c) shows the Fe 2p spectra for Fe_2O_3 and each of the Fe-CeO_2 composites. Two distinct peaks at binding energies of 711.5 eV and 725.3 eV corresponded to Fe $2p_{3/2}$ and Fe $2p_{1/2}$, respectively and an additional satellite peak is present at 719.5 eV further confirming the presence of Fe^{3+} and were all in good agreement with values reported for Fe_2O_3[67] and confirmed that surface iron present in the samples is in the +3 valence state.[68] A shift of the Fe $2p_{3/2}$ peak to lower binding energies was observed with decreasing Fe content in the solid solution catalysts and was attributed to Fe-Ce interactions in the solid solution catalysts, specifically an increase of electron density occurring with a smaller concentration of Fe^{3+} within the lattice from the 2:1 to 1:2 samples. The Fe 3p spectra, shown in **Figure S5** a) was in agreement with the literature for Fe_2O_3[67] and similar to the Fe2p core level, a slight shift to lower binding energies was observed for the solid solutions which was also attributed to Fe-Ce electronic interactions.

The O1s spectra for the Fe_2O_3, CeO_2, and Fe-CeO_2 solid solutions are shown in **Figure S5** b). The peak at a BE of ~529 eV for each of the samples was assigned to the metal-oxygen (M-O) or O^{2-} species within the structure. The peak at a higher binding energy of ~531 eV is assigned to oxygen defects, commonly reported for transition metal oxide species and are indicative of regions where the coordination number of O is smaller than in regular sites.[69] The formation of oxygen defects within the lattice structure as well as an increase in Ce^{3+} sites is attributed to the reduction of particle size on incorporation of Fe into the CeO_2 lattice and can contribute to enhanced oxygen mobility or improved redox properties of the catalyst.[46] A third peak arising at ~533 eV was assigned to surface hydroxides which may arise from water adsorption and is in agreement with the literature.[70]



Catalyst	Ce^{3+}	Ce^{4+}
CeO_2	20 %	80 %
Fe-CeO_2 1:2	52 %	48 %
Fe-CeO_2 1:1	44 %	56 %
Fe-CeO_2 2:1	58 %	42 %

Figure 2: a) Ce 3d core level XPS spectrum for CeO_2 and the Fe-CeO_2 solid solutions b) quantitative data from the Ce3d core level scans and c) Fe 2p core level XPS spectrum for Fe_2O_3 and the Fe-CeO_2 solid solutions.

SEM was used to assess the morphology of the Fe-CeO_2 solid solution catalysts as shown in **Figure 3** a)-c) showing needle-like nanostructures. Ceria nanorods have been reported to have superior catalytic properties for water-gas shift reaction over other ceria morphologies owing to a higher lattice strain resulting in increased oxygen vacancies.[71] Another study reported ceria nanorods to have higher Ce^{3+} content leading to increased oxygen vacancies and therefore enhanced activity for the hydrogenation of cinnemaldehyde.[72] EDX analysis of the Fe-CeO_2 1:1 catalyst is shown in **Figure 3** d) and illustrates an even dispersion of Fe and Ce throughout the sample. Further EDX mapping was carried out using HAADF-STEM for the Fe-CeO_2 2:1, 1:1 and 1:2 catalysts which is shown in the Supplementary Information **Figure S6**. The EDX maps show the Fe is uniformly dispersed in catalysts with a Fe-CeO_2 molar ratio of 1:1 and 1:2, while the catalyst with molar ratio 2:1 shows some segregated Fe regions, attributed to the presence of Fe_2O_3, in good agreement with the XRD and Raman analysis. This observation is also confirmed by high resolution TEM analysis, as shown in **Figure 3** e)-j). TEM images of each of the catalysts (e)-g)) shows the formation of aggregates of small diameter nanoparticles. The mean particle diameter and standard deviations were approximated from the images to be 5.3 ±1.2 nm (Fe-CeO_2 1:2), 4.9 ± 1.7 nm (Fe-CeO_2 1:1) and 3.8 ± 0.8 nm (Fe-CeO_2 2:1) and the size distribution histograms are shown in SI **Figure S7**. **Figure 3** h)-j) shows the HRTEM of each of the catalyst with the FFT of each in the inset of the images. The Fe-CeO_2 1:2 solid solution confirms the presence of cubic fluorite ceria from the presence of the (200), (111) and (220) lattice fringes with *d*-spacing of 0.298 nm, 0.340 nm and 0.170 nm, respectively.[73] The inset shows four strong rings assigned to the (111), (200), (220) and (311) crystal planes of crystalline cubic fluorite ceria ($Fm\bar{3}m$). The Fe-CeO_2 1:1 catalyst showed lattice fringes with *d*-spacings of 0.336 nm, 0.211 nm and 0.168 nm which were assigned to the (111), (200) and (220) CeO_2 planes. A decrease in the *d*-spacing for the Fe-CeO_2 1:1 catalyst compared to the Fe-CeO_2 1:2 samples can be attributed to the shrinkage of the CeO_2 lattice on an increase of Fe content.[74] The *d*-spacing for the Fe-CeO_2 2:1 catalyst, illustrated in in **Figure 3** j), shows the CeO_2 (111) *d*-spacing further decreases to 0.327 nm, evidencing shrinkage of the ceria lattice due to Fe incorporation. The Fe-CeO_2 2:1 sample is the only sample that showed the presence of an Fe_2O_3 crystal plane with a *d*-spacing of 0.376 nm, which was assigned to the (012) plane of hexagonal Fe_2O_3 and further supports the Raman and XRD analysis. The FFT pattern shows the formation of Fe_2O_3 with a hexagonal lattice showing the (104), (012) and (110) planes.[75, 76]

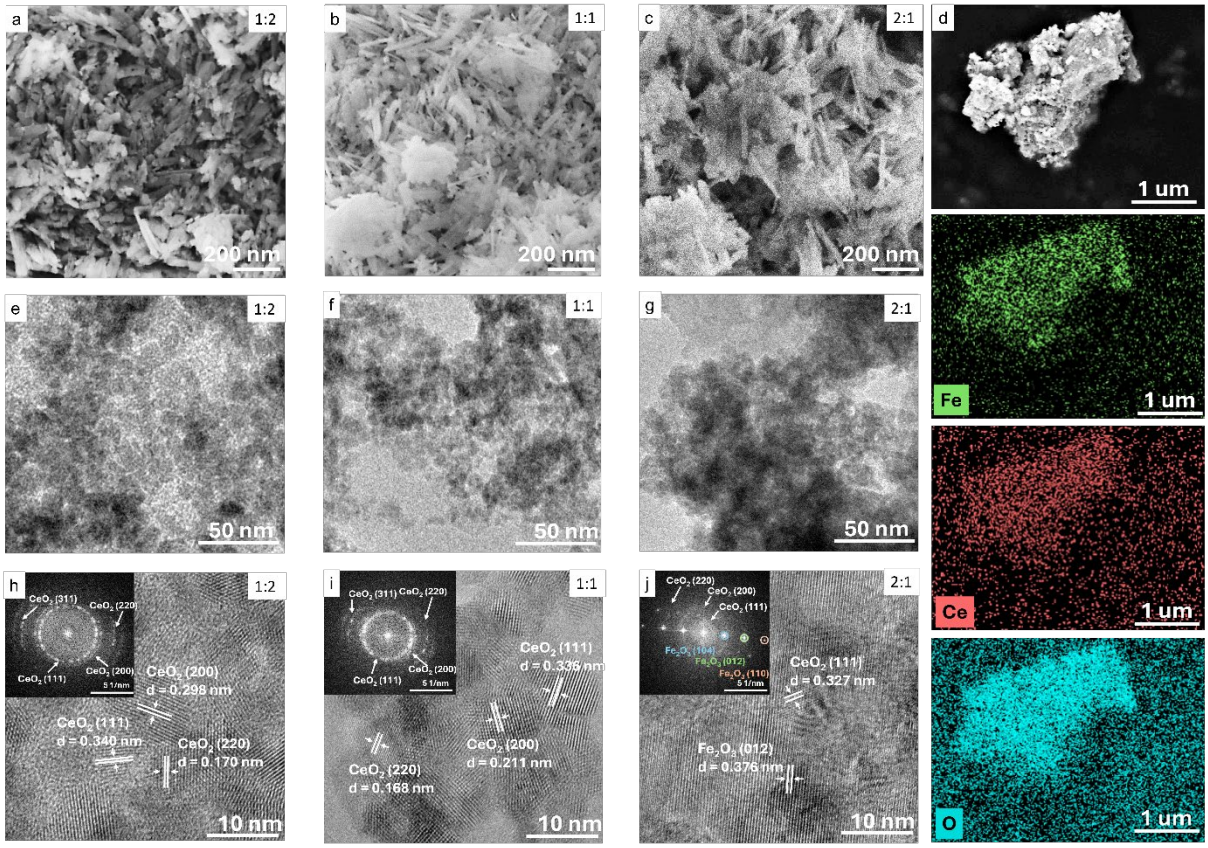


Figure 3: a)-c) SEM images of Fe-CeO_2 catalyst with Fe:Ce molar ratios of 1:2, 1:1 and 2:1, d) SEM and corresponding EDX of Fe-CeO_2 1:1, e)-g) TEM images of Fe-CeO_2 1:2, 1:1 and 2:1, h)-j) HRTEM with FFT of Fe-CeO_2 1:2, 1:1 and 2:1.

Figure S8 a) shows the total reflection X-ray fluorescence (TXRF) spectra for each solid solution catalyst, which was used to further quantify Fe and Ce in the catalysts. The spectrum shows peaks assigned to the emission lines of $L_{\alpha1}$, $L_{\beta1}$, $L_{\gamma1}$ and $L_{\gamma2}$ for Ce and of $K_{\alpha1}$ and $K_{\beta1}$ for Fe. The quantitative data is shown in **Table S1** and confirmed that molar ratios of Fe and Ce in each Fe-CeO_2 catalyst was in excellent agreement with the precursor ratio used in the synthesis.

2.2 Catalytic evaluation of Fe-CeO_2 solid solution catalyst for oxidative degradation of polyethylene

The Fe-CeO_2 solid solutions were tested as heterogeneous Fenton-type catalysts in the microwave-assisted oxidative degradation of LDPE with the aim of maximising the yield of organic acids. The use of microwave assisted heating has many benefits over conventional thermal heating due to the uniform heat transfer and rapid volumetric heating which has been shown to increase reaction rates and higher product yields in reactions involving chemical plastic degradation.[77, 78] While a specific microwave-assisted Fenton mechanism has not yet been proposed, the reactivity under MW-assisted

heating is likely due to the use of catalytic metals with high microwave absorbing properties as well as a polar solvent with a high dielectric constant contributing to specific "hot spots" being created at catalyst-solvent interfaces.[52, 79, 80] The degradation products were identified and quantified using HPLC by establishing calibration curves for eight acid standards: succinic acid, formic acid, glutaric acid, acetic acid, adipic acid, propionic acid, butyric acid and pimelic acid, shown in **Figure S9** a). The retention times of each standard are shown in **Figure S9** b) and a typical chromatogram of the degradation products is shown in **Figure S9** c).

Initially, the reactions were carried out using typical Fenton conditions such as acidic solution (pH 1) and an catalyst mass loading of 10 wt. %.[32, 34] A mass of 0.3 g LDPE was used along with 10 mL of a H_2O_2 solution 9 % (w/w). The reproducibility of the reactions over three reactions was approximated to be within an error of ±10 %. **Figure 4** a) shows the effect of temperature and stir speed on the reaction efficiency. The mass loss for LDPE shows an almost linear response to temperature increasing from 20% at 150 °C to 90 % at 180 °C. The reaction also favored high stir speeds, attributed to the hydrophobic surface of the LDPE and the heterogeneous nature of the reactions. Optimal microwave reaction conditions were 180 °C for 3 h with 1900 rpm stir speed. **Figure 4** b), shows the performance of the Fe-CeO_2 solid solution catalysts as well as Fe_2O_3 and CeO_2. While both Fe_2O_3 and CeO_2 both act as catalysts under these conditions, the combined use of Fe-CeO_2 as the catalyst gave higher mass loss and yields, indicating a synergistic effect between the Fe and CeO_2. Synergistic effects in multi-metal Fenton catalysts have been reported to be attributed to the presence of multivalent ions which play distinct roles in the catalytic mechanism.[81] In the reaction, the lower valent metal (Ce^{3+}, Fe^{2+}) nucleophilically attacks the O-O bond of the H_2O_2 to generate a hydroxy radical ($^{\bullet}OH$) and, the higher valent metal (Ce^{4+}, Fe^{3+}) electrophilically abstracts the H from the H_2O_2 generating hydroperoxyl radicals ($HO_2^{\bullet}$)[81] . The Fe-CeO_2 2:1 and Fe-CeO_2 1:2 catalysts had similar activity with mass losses of 81 % and 74 % and yields of 63 % and 60 %, respectively. They were both outperformed by the Fe-CeO_2 1:1 catalyst with a 94% mass loss and 78 % yield. The Fe-CeO_2 2:1 catalyst may be less effective due to aggregates of iron oxides disrupting the synergistic effect of the solid solution structure. The Fe-CeO_2 1:2 catalyst may be less effective due to the lower Fe content.[46]

As it was the best performing catalyst, Fe-CeO_2 1:1 was used to study the effect of the H_2O_2 concentration and catalyst loading on both the mass loss and acid yield. **Figure 4** c) illustrates the interplay between H_2O_2 concentration and catalyst loading. When using 10 wt. % catalyst loading, the mass loss and yield increased linearly with the H_2O_2 concentration and excellent performance was observed using 9 % (w/w) H_2O_2 with a mass loss LDPE of 94 % and an acid yield of 78 %. At very high catalyst loading of 30 wt. % full mass loss is observed but the organic acid yield decreases with increasing H_2O_2 concentration due to over-oxidation of the acid products to gaseous reagent such as

CO_2. This indicates that catalyst system could be tuned to gaseous products which has been a strategy used for the destruction of microplastics. [22]

One key advantage of heterogeneous Fenton systems over homogeneous Fenton systems is their operation over a wide pH range.[26] The effect of solution pH was evaluated for the Fe-CeO_2 1:1 catalyst at a pH of 1, 4 and 7 and the results are shown in **Figure 4** d). While a trend of decreased yield with increasing pH was noted, good catalytic activity at neutral pH was still observed, with a mass loss of 77% and acid yield of 55 %. The main product found for the reaction at pH 1 was butyric acid, while formic acid was the main product for the reaction at pH 4 and pH 7 indicative of mechanistic differences in the degradation process. The different reaction products under acidic conditions may be attributed to the presence of nitric acid contributing to LDPE degradation and oxidation through the formation radicals from HNO_3 under MW irradiation.[22] Implementing the oxidative degradation reaction at a neutral pH is more favorable as a safer and greener reaction protocol. Additionally, removing the use of nitric acid limits the formation of unwanted nitrate contaminants in the product mixture.[21] HPLC analysis of the product shown in Supplementary Information **Figure S10** show a significant decrease in the nitrate peak intensity when nitric acid was not added to the reaction mixture. A minor nitrate peak is still present due to the use of nitrate stabilizers in both H_2SO_4 and H_2O_2.

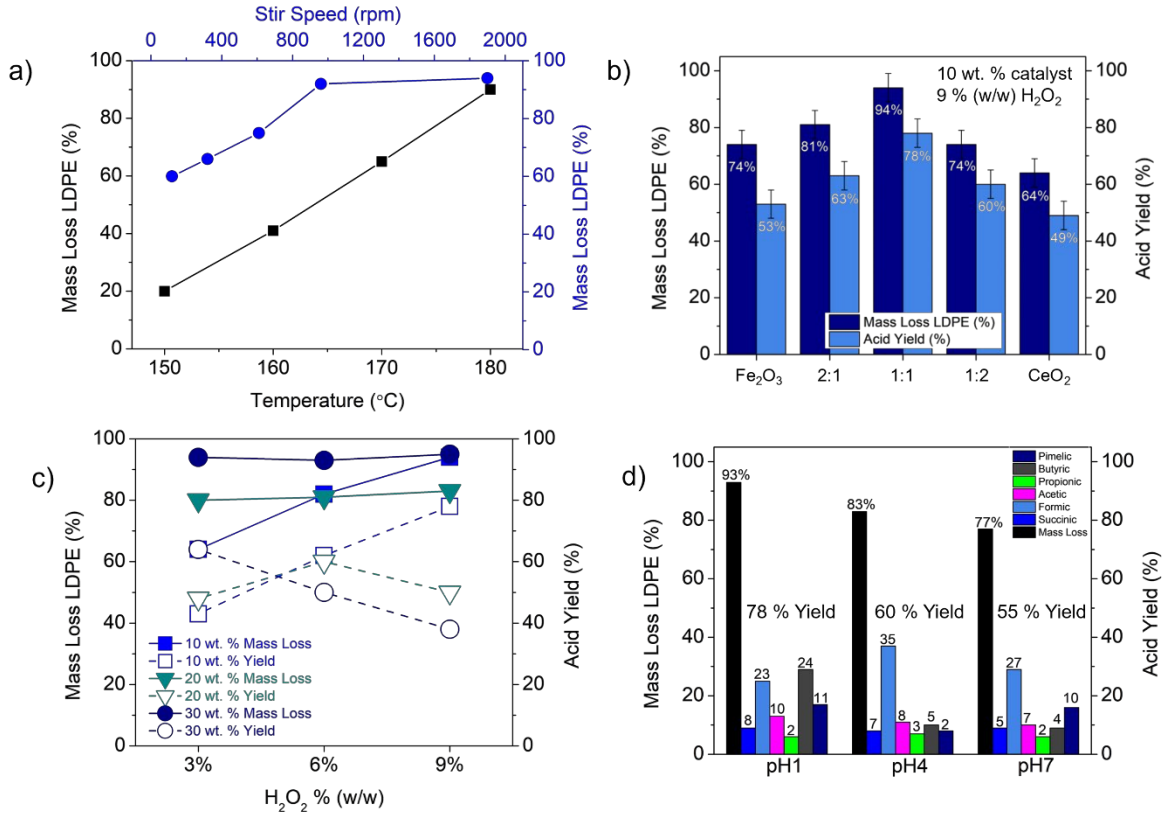


Figure 4: a) effect of stir speed and temperature on mass loss LDPE (0.3 g LDPE, pH 1, 10 wt. % catalyst loading (0.03 g), 10 mL 9 % H_2O_2), b) catalyst screening at pH1 (0.3 g LDPE, 10 wt. % catalyst loading (0.03 g), 10 mL 9 % H_2O_2 (w/w), c) effect of H_2O_2 concentration and catalyst loading on acid yield (0.3 g LDPE, pH 1), d) catalytic results at pH 1, 4 and 7 with product distribution (0.3 g LDPE, 10 wt. % catalyst loading (0.03 g), 10 mL 9 % H_2O_2).

2.3 Catalytic Optimization of Polyethylene Degradation under Neutral pH

The Fenton catalytic degradation of LDPE at neutral pH is highlighly advantageous, so these conditions were further optimized to maximize the organic acid yield at pH 7 and evaluate the product composition. For the screening study, 0.5 g of LDPE, Fe-CeO_2 1:1 catalyst with loadings ranging from 1 – 15 wt. % were used with 10 mL solutions of H_2O_2 ranging from 5 – 15 % (w/w). **Figure 5** a) shows the LDPE mass loss and total organc acid yield as a function of H_2O_2 concentration when using different catalyst loadings (1, 5 and 10 wt. %) under netural pH and illustrate that both catayst loading an H_2O_2 concentration play a crucial role in determining the mass loss and organic acid yield. From **Figure 5** it can be seen that at lower H_2O_2 concentration (5 w/w %) the mass loss increases with the increasing catalyst loading, yet the yield of the organic acid remained similar. As the H_2O_2 concnetration is increased to 10 w/w % all catalysts showed higher mass losses and yields. The effect of further increases in H_2O_2 concentration was dependent on catalyst loading. When using 10 wt% catalyst loading under neutral pH, the mass loss and yield both decreased suggesting catalyst deactivation under these reaction conditions. A well reported deactivation mechanism with increased catalyst loading in heterogeneous systems is catalyst deactivation due to agglomeration.[82] Decreased mass loss and yield were not observed for the reactions carried out acidic conditions even under high loading conditions likely owing to the presence of nitric acid contributing to degradation of the LDPE.

Figure 5 illustrates that under neutral reaction conditions lower catalyst loadings with higher H_2O_2 concentrations are optimal to the achieve simultaneous high mass loss and high organic yields. For example, at 1 wt% catalyst loading and 5 % w/w H_2O_2, the mass loss of LDPE was only 41% (19 % yield), but this increased to a mass of 91% and yield of 71 % using 15% w/w H_2O_2. **Figure 5** b) illustates the organic acid yields and product distributions as a function of the catalyst loading and H_2O_2 concentration. The dominant products present at low H_2O_2 concentrations are succinic, formic, acetic and propionic acid. As H_2O_2 concentrations increase, the formation of longer chain acids, pimelic, glutaric, and butyric acid is observed in the mixtures. While butyric acid was the dominant acid formed under pH 1, at pH 7 butyric acid was absent or only a minor conponent of the acid mixture.

Shown in Supplementary Information **Figure S11**, the reaction carried out in the absence of a catalyst (0.5 g LDPE and 10 mL H_2O_2 15 % (w/w)) gave a 15 % mass LDPE loss and 8 % acid yield. The reaction carried out in the absence of H_2O_2 (0.5 g LDPE, 1 wt. % catalyst 10 mL H_2O) gave a mass loss of 10 % and an acid yield of 8 %. These results show the importance of the presence of both catalyst and H_2O_2 in the reaction.

The Fe-CeO_2 solid solution catalysts of different molar ratios as well as Fe_2O_3 and CeO_2 catalysts were then screened again at the optimized pH 7 conditions (1 wt. % catalyst loading 10 mL 15 % H_2O_2 (w/w) shown in **Figure 5** c). A similar synergistic effect was observed at pH 7 as was observed with reaction carried out at pH 1. All the solid solution catalysts display good activity, as shown in **Figure** 5 c) but the Fe-CeO_2 1:1 catalyst was again found to be the best performing. The catalyst performance of CeO_2 was relatively poor under neutral conditions (mass loss 41 %, yield 15 %). The redox cycle of Ce^{4+} to Ce^{3+} has been reported to form cerium-peroxide complexes ($\equiv Ce^{3+}$-OOH) which are stable at pH 7 and therefore do not degrade to radicals.[83] The good performance of the solid solution catalysts relative to CeO_2 at neutral pH suggests that when Ce is in the form of Fe-CeO_2 solid solution structure, the cerium-peroxide complexes are not as stable or may not form at all, another benefit of the solid solution catalyst structure.

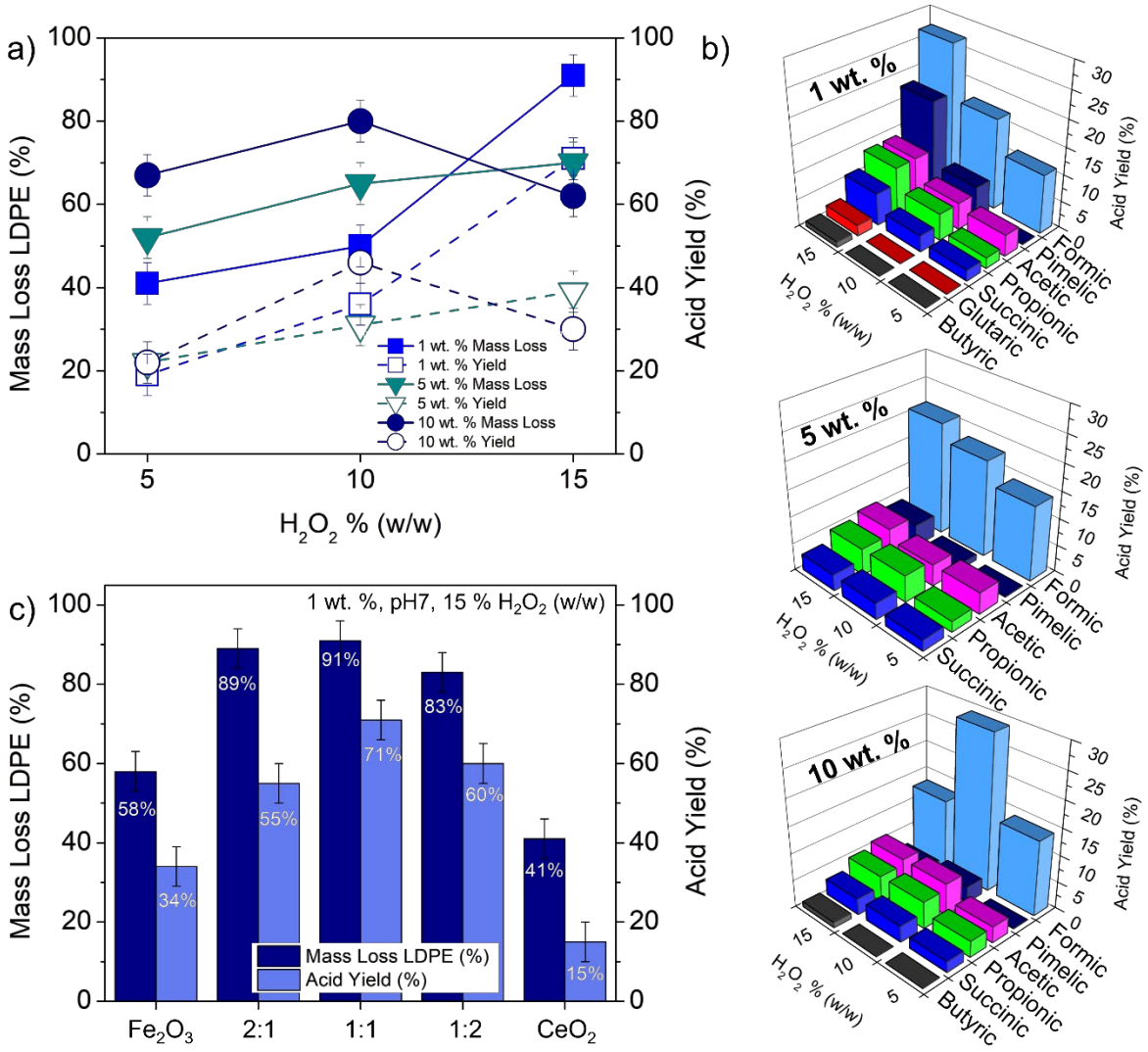


Figure 5: a) effect of H_2O_2 concentration and catalyst loading on mass loss and acid yield at pH 7 (0.5 g LDPE), b) effect of catalyst loading and H_2O_2 concentration on product distribution at 1 wt. %, 5 wt. % and 10 wt. % catalyst loading, and 5, 10 and 15 % (w/w) H_2O_2, respectively, c) catalyst screening at optimised conditions (0.5 g LDPE, 1 wt. % catalyst loading, 10 mL 15 % H_2O_2 (w/w), pH 7).

2.4 Reaction Time Series

A time series was carried out to evaluate the products formed in the oxidative degradation process of LDPE after 1 h, 2 h and 3 h of reaction time. **Figure 6 a)** shows the mass loss and yield for the Fe-CeO_2 catalyst with different molar ratios which all increase linearly with time. The Fe:Ce molar ratio clearly plays a role in catalytic efficiency in terms of mass loss and organic acid yield. The Fe-CeO_2 catalyst with molar ratio of 1:1 resulted in the highest mass loass and acid yields. **Figure 6 b)** shows the reaction product distributions obtained from each catalyst over the reaction. The intial degradation products

were succinic acid, formic acid and acetic acid and similar for all catalysts. The formation of longer chain acids, propionic acid, and pimelic acid and small amouts of glutaric and butyric acid was observed in each product mixture as the reaction proceeded. After 3 h of reaction time, the highest yields were obtained with the Fe-CeO_2 1:1 catalyst. Interestingy, a larger amount of pimelic acid (18 %) was observed in the Fe-CeO_2 1:1 product mixture relative to the Fe-CeO_2 2:1 (6 %) and the Fe-CeO_2 1:2 (9 %) catalysts. While the origin of the pimelic acid is not clear, it is likely due to the optimised tuning of the ratio of Fe and Ce in the catalyst. While the mechanisms are not comparable, high yields of pimelic acid have also previously been reported for thermal aerobic oxidation with molecular oxygen[84], and NO_x/O_2 systems.[85] FTIR analysis of the LDPE after 1 h, 2 h and 3 h reaction times is showin in **Figure 6** c) and identified the formation of C=O and C-O groups due to surface oxidation of the polymer from attack of $HO^{\bullet}$ and $HO_2^{\bullet}$ radicals in solution. The carbonyl index was measured to be 0.85, 1.78 and 4.40 for the 1 h, 2 h and 3 h residual LDPE respectively. SEM images in **Figure 6** d) show the physical change in surface texture of the LDPE with an increase in surface roughness during the reaction. Small pore-like structures of approximately 5 µm diameter were observed after 1 h of reaction time and an increase in surface roughness of the over time is clearly observed. Additionally, an increase in surface oxygen can be observed from the EDX elemental mapping as the reaction proceeds, correlating with the FTIR analysis. XPS analysis of the residual LDPE surface after 3 h of reaction time shown in Supplementary information **Figure S12** and showed four peaks at 284.7 eV, 285.4 eV, 286.9 eV and 288.8 eV which were attributed to C-C, C-O, C=O and O-C=O species on the LDPE surface, respectively.[86]

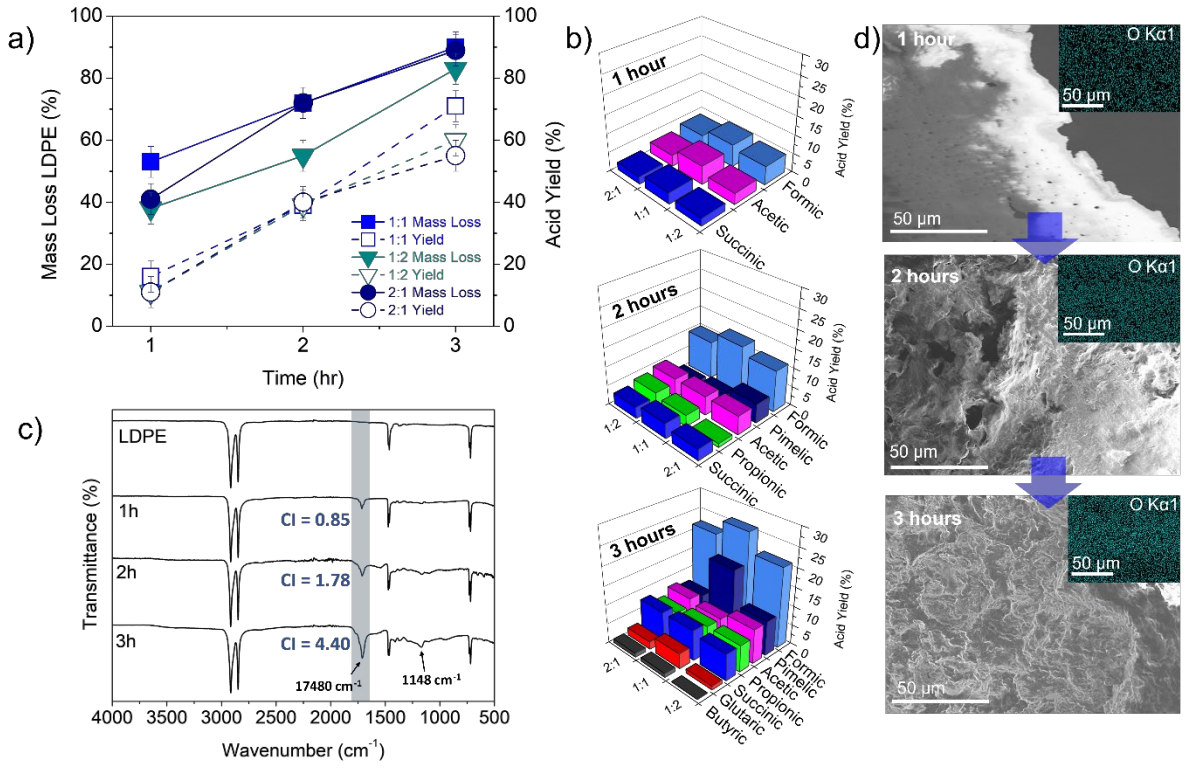


Figure 6: a) Time series results for Fe-CeO_2 1:2, 1:1 and 2:1 catalysts (0.5 g LDPE 1 wt. % catalyst, 15 % (w/w) H_2O_2), b) product distribution, c) FTIR analysis of LDPE residue surface after 1h, 2h and 3h reaction times with carbonyl index (CI), d) SEM of LDPE residue surface with oxygen EDX maps after 1h, 2h and 3h of reaction time.

2.5 Catalytic Recyclability

The results of the recyclability performance test of the Fe-CeO_2 1:1 catalyst are shown in **Figure 7** a). The catalyst was found to be effective over 6 cycles with no loss in acid yield over each cycle. The superior recyclability performance can be accredited to the conservation of of Ce^{4+} and Ce^{3+} ratio as determined by XPS shown in **Figure 7 b)** and no signifcant leaching of the Fe. TXRF (shown in Supplementary Information **Figure S13** analysis confirmed the preservation of the 1:1 Fe:Ce molar ratio of the catalyst after 6 cycles. The high recycability performance was attributed to the ability of the solid solution structure to retain the 1:1 Fe:Ce molar ratio as no Fe sludge leaching was evident as it was after reactions using Fe_2O_3.

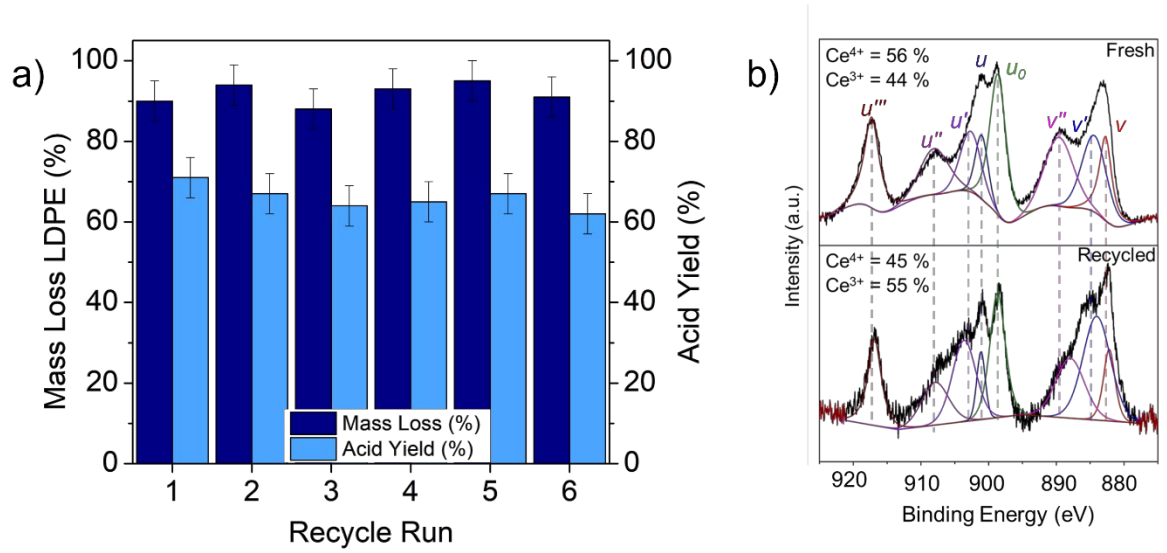


Figure 7: a) Recyclability performance of catalyst (0.5 g LDPE, 1 wt. % catalyst, 15 % (w/w) H_2O_2, 3 h, 180 °C, b) Ce 3d XPS of fresh and recycled catalyst.

Due to the complex nature of the oxidation process, Fenton oxidation mechanisms are still being proposed for heterogeneous systems. However, the catalytic efficiency and recyclability of the Fe-CeO_2 catalyst at neutral pH can almost certainly be attibuted to its solid solution structure. Metal leaching from various heterogeneous iron oxide Fenton catalysts under these reaction conditions is well known which is highly unfavourable due to metal contamination of the product mixture.[26, 87]

The heterogeneous Fenton mechanism is not fully understood owing to multiple reaction pathways, different coordination chemistries between H_2O_2 and metal catalysts and difficulty tracking the short-lived radical complexes that form in the reaction. However, a compilation of the accepted general mechanisms for heterogeneous Fe and Ce at acidic and neutral pH are summarized in **Table 1**. The decomposition rate of H_2O_2 in heterogeneous Fenton chemistry is said to be proportional to the concentration of H_2O_2 and the surface area of the catalyst.[88] The heterogeneous Fe mechanism at acidic pH is shown in table entry 1 and involves the adsorption of H_2O_2 on to the Fe^{3+} surface. This is subsequently followed by the formation of surface Fe^{2+} and a superoxide species owing to electron transfer from peroxide ligand to metal species. This leads to the formation of $HO^{\bullet}$ radicals which can interact with H_2O_2 and undergo chain reactions resembling homogeneous Fenton processes. Similarly, at acidic pH, cerium is proposed to form Ce/H_2O_2 complexes shown in entry 2 which subsequently degrade to $HO^{\bullet}$ and $HO_2^{\bullet}$ by an electron transfer pathway.

The widely accepted heterogeneous Fenton mechanism for Fe^{3+} (goethite) at neutral pH is shown in entry 3. The interaction of the Fe^{3+}-OH catalyst surface with H_2O_2 forms a stabilized H_2O_2 complex

referred to as $(H_2O_2)_s$. A ligand-to-metal charge transfer then results in the formation of and Fe^{2+} transition state complex which then dissociates to form a $HO_2^{\bullet}$ radical. The regeneration of Fe^{3+} in the system then leads to the subsequent formation of $HO^{\bullet}$ radicals. In comparison, CeO_2 is not as effective Fenton heterogeneous catalysts at neutral pH due to the formation of stable Ce/H_2O_2 complexes which do not degrade to radicals at pH 7 shown in entry 4, but the benefical effect between Fe and Ce, plays an important role in the activity of Fe-CeO_2 solid solution catalyst.

Studies using in-situ electron spin resonance spectroscopy to assess radical formation in Fe/Ce systems have reported the predominantly active species to be $^{\bullet}OH$[89, 90]. Although the heterogeneous Fenton mechanism is exceptionally complex, literature has broadly defined the radical cycle in a series of 3 simple equations. The initiation step (Eqn. 1) of the Fenton reaction can generally be defined as the generation of $^{\bullet}OH$ from the redox decomposition of H_2O_2 over a Fenton catalyst (Fe, Ce). In the propagation step (Eqn. 2), the generated $^{\bullet}OH$ subsequently oxidises the LDPE chain which occurs through its own series of initiation, propagation and termination reactions. Termination (Eqn. 3) of the $^{\bullet}OH$ radical occurs when it comes into contact with the Fenton catalyst again, oxidising it and forming ^{-}OH as a result.[91, 92]

$$H_2O_2 + Fe^{2^+} \rightarrow Fe^{3^+} + HO^{\bullet} + HO^{-} \quad \textbf{Eqn. 1}$$

$$RHR' + HO^{\bullet} + HO^{-} \rightarrow ROHR' + H_2O \quad \textbf{Eqn. 2}$$

$$HO^{\bullet} + Fe^{3^+} \rightarrow Fe^{2^+} + HO^{-} \quad \textbf{Eqn. 3}$$

Nguyen *et al.*[37] proposed a multi-step Fenton oxidation mechanism of polyethylene by mechano-catalytic cracking, followed by C-C clevage in the PE chain. The reaction equations are described in Table 1 entry 5. Radicals produced from the heterogeneous Fenton mechanism form a secondary alcohol species. Further oxidation by radical attack leads to formation of a ketone susceptible to further oxidation via Baeyer-Villigar oxidation to an ester group. This is followed by hydrolysis of the ester group to a carboxylic acid. Terminal alcohol groups can also be oxidised to a carboxylic acid. Formic and acetic acid have been reported as the main oxidation products from polyethylene.[93]

Table 1: Redox Cycles of Fe and Ce under acidic and neutral pH and proposed mechanism of oxidation of PE based on literature reports.

Mechansim	Equation	Ref
1. Heterogeneous Fe (acidic pH)	$H_2O_2 + \equiv Fe^{3+} \leftrightarrow \equiv Fe^{3+}(O_2H) + H^+$	[88]

	$\equiv Fe^{3+}(O_2H) \rightarrow \equiv Fe^{2+} + HO_2\cdot/(O_2\cdot^- + H^+)$ $\equiv Fe^{2+} + H_2O_2 \rightarrow \equiv Fe^{3+} + HO^\bullet + OH^-$ $H_2O_2 + HO^\bullet \rightarrow HO_2\cdot/(O_2\cdot^- + H^+) + H_2O$	
2. Heterogeneous Ce (acidic pH)	$\equiv Ce^{4+} + H_2O_2 \rightarrow \equiv Ce^{4+}(O_2H) + H^+$ $\equiv Ce^{4+}(O_2H) \rightarrow \equiv Ce^{3+} + HO_2\cdot$ $\equiv Ce^{3+} + H_2O_2 \rightarrow \equiv Ce^{4+} + HO^\bullet + OH^-$	94
3. Heterogeneous Fe (neutral pH)	$\equiv Fe^{3+} - OH + H_2O_2 \leftrightarrow (H_2O_2)_s$ $(H_2O_2)_s \leftrightarrow (\equiv Fe^{2+\bullet}O_2H) + H_2O$ $(\equiv Fe^{2+\bullet}O_2H) \rightarrow \equiv Fe^{2+} + HO_2\cdot$ $\equiv Fe^{2+} + H_2O_2 \rightarrow \equiv Fe^{3+} - OH + {}^\bullet OH$	95
4. Heterogeneous Ce (neutral pH)	$\equiv Ce^{4+} + H_2O_2 \rightarrow \equiv Ce^{4+}(O_2H) + H^+$ $\equiv Ce^{4+}(O_2H) \nrightarrow$	94, 96
5. Oxidation of PE	**1. Heterogeneous Fenton** $RHR' + H_2O_2 \rightarrow ROHR' + H_2O$ **2. Oxidation** $ROHR' + H_2O + H_2O_2 \rightarrow RCOR' + 2H_2O$ **3. Baeyer-Villiger Oxidation** $RCOR' + H_2O_2 \rightarrow RCOOR' + H_2O$ **4. Hydrolysis** $RCOOR' + H_2O \rightarrow \boldsymbol{RCOOH}$ **5a. Oxidation** $ROH + H_2O_2 \rightarrow RCOH + 2H_2O$ **5b. Oxidation** $RCOH + H_2O_2 \rightarrow \boldsymbol{RCOOH} + H_2O$ **Over-oxidation to gaseous products:** $RCOH \rightarrow CO\uparrow + RH$	37, 96

	$RCOOH \rightarrow CO_2 \uparrow + RH$ **Decarbonylation / Radical Transfer**	

3. Conclusions

This work demonstrates that the microwave-assisted oxidative degradation of LDPE can be effectively tuned to obtain a mixture of carboxylic acid products limiting over-oxidation to gaseous products. The heterogeneous Fenton process was proven successful at neutral pH which is favourable as no acid addition is required minimising undesirable side products. No pre-treatment was required for the LDPE, allowing for a one-step degradation process. The synergistic effect, specifically the redox cycle of iron and cerium and the importance of tuning their molar ratios in the system has been demonstrated with the Fe-CeO_2 1:1 achieving the highest LDPE mass loss of 91% and organic acid yields of 71% at neutral pH. The excellent recyclability of the catalyst was attributed to the solid solution structure which allowed for the preservation of Fe and Ce in a 1:1 ratio as well as the preservation of optimal ratios of Ce^{3+} and Ce^{4+} after 6 cycles. The main products obtained were formic acid as well as acetic acid, succinic acid and pimelic acid which are all valuable polymer precursors. Overall, the work shows that the Fe-CeO_2 solid solution catalyst performs exceptionally as a Fenton-type heterogeneous catalyst, providing a valuable pathway for the oxidative degradation of LDPE to valuable products.

Conflicts of interest

There are no conflicts to declare.

Acknowledgements

We acknowledge Science Foundation Ireland grant number (AMBER Grant No: 12/RC2278_P2). We thank the Advanced Microscopy Laboratory at Trinity College Dublin for TEM analysis, Bernal Institute University of Limerick for access to XPS facilities and Tyndall National Institute for access to SEM and XRD facilities.

References:

1. J. Hopewell, R. Dvorak and E. Kosior, *Philosophical Transactions of the Royal Society B: Biological Sciences*, 2009, **364**, 2115-2126.
2. P. He, L. Chen, L. Shao, H. Zhang and F. Lü, *Water Research*, 2019, **159**, 38-45.
3. D. K. A. Barnes, F. Galgani, R. C. Thompson and M. Barlaz, *Philosophical Transactions of the Royal Society B: Biological Sciences*, 2009, **364**, 1985-1998.
4. R. Meys, F. Frick, S. Westhues, A. Sternberg, J. Klankermayer and A. Bardow, *Resources, Conservation and Recycling*, 2020, **162**, 105010.
5. J. Jiang, K. Shi, X. Zhang, K. Yu, H. Zhang, J. He, Y. Ju and J. Liu, *Journal of Environmental Chemical Engineering*, 2022, **10**, 106867.
6. J. Huang, A. Veksha, W. P. Chan, A. Giannis and G. Lisak, *Renewable and Sustainable Energy Reviews*, 2022, **154**, 111866.
7. Y. Liu, J. Shi, H. Jin and L. Guo, *Environmental Chemistry Letters*, 2024, **22**, 149-169.
8. M. Watanabe, Y. Matsuo, T. Matsushita, H. Inomata, T. Miyake and K. Hironaka, *Polymer Degradation and Stability*, 2009, **94**, 2157-2162.
9. W. Stuyck, K. Janssens, M. Denayer, F. De Schouwer, R. Coeck, K. V. Bernaerts, J. Vekeman, F. De Proft and D. E. De Vos, *Green Chemistry*, 2022, **24**, 6923-6930.
10. É. Casey, R. Breen, J. S. Gómez, A. P. M. Kentgens, G. Pareras, A. Rimola, J. D. Holmes and G. Collins, *ACS Sustainable Chemistry & Engineering*, 2023, **11**, 15544-15555.
11. T. Thiounn and R. C. Smith, *Journal of Polymer Science*, 2020, **58**, 1347-1364.
12. R. Geyer, J. R. Jambeck and K. L. Law, *Sci Adv*, 2017, **3**, e1700782.
13. The Round Up Plastic Waste Statistics, https://theroundup.org/plastic-waste-statistics/).
14. S. D. Anuar Sharuddin, F. Abnisa, W. M. A. Wan Daud and M. K. Aroua, *Energy Conversion and Management*, 2016, **115**, 308-326.
15. M. Solis and S. Silveira, *Waste Management*, 2020, **105**, 128-138.
16. A. Piovano and E. Paone, *Current Research in Green and Sustainable Chemistry*, 2022, **5**, 100334.
17. R. Cao, M.-Q. Zhang, C. Hu, D. Xiao, M. Wang and D. Ma, *Nature Communications*, 2022, **13**, 4809.
18. S. Oh and E. E. Stache, *Journal of the American Chemical Society*, 2022, **144**, 5745-5749.
19. K. P. Sullivan, A. Z. Werner, K. J. Ramirez, L. D. Ellis, J. R. Bussard, B. A. Black, D. G. Brandner, F. Bratti, B. L. Buss, X. Dong, S. J. Haugen, M. A. Ingraham, M. O. Konev, W. E. Michener, J. Miscall, I. Pardo, S. P. Woodworth, A. M. Guss, Y. Román-Leshkov, S. S. Stahl and G. T. Beckham, *Science*, 2022, **378**, 207-211.
20. Z. Xu, N. E. Munyaneza, Q. Zhang, M. Sun, C. Posada, P. Venturo, N. A. Rorrer, J. Miscall, B. G. Sumpter and G. Liu, *Science*, 2023, **381**, 666-671.
21. K. Pinsuwan, P. Opaprakasit, A. Petchsuk, L. Dubas and M. Opaprakasit, *Polymer Degradation and Stability*, 2023, **210**, 110306.
22. E. Bäckström, K. Odelius and M. Hakkarainen, *Industrial & Engineering Chemistry Research*, 2017, **56**, 14814-14821.
23. Y. Wang, P. Gao, Y. Wei, Y. Jin, S. Sun, Z. Wang and Y. Jiang, *Journal of Environmental Management*, 2021, **278**, 111473.
24. S. Ziembowicz and M. Kida, *Chemosphere*, 2022, **296**, 134041.
25. D. Meyerstein, *Nature Reviews Chemistry*, 2021, **5**, 595-597.
26. N. Thomas, D. D. Dionysiou and S. C. Pillai, *J Hazard Mater*, 2021, **404**, 124082.
27. M. A. Fontecha-Cámara, C. Moreno-Castilla, M. V. López-Ramón and M. A. Álvarez, *Applied Catalysis B: Environmental*, 2016, **196**, 207-215.
28. P. V. Nidheesh, *RSC Advances*, 2015, **5**, 40552-40577.
29. X. Wang, R. Yin, L. Zeng and M. Zhu, *Environmental Pollution*, 2019, **253**, 100-110.

30. C. Lai, X. Shi, L. Li, M. Cheng, X. Liu, S. Liu, B. Li, H. Yi, L. Qin, M. Zhang and N. An, *Science of The Total Environment*, 2021, **775**, 145850.
31. N. d. O. Dos Santos, R. Busquets and L. C. Campos, *Science of The Total Environment*, 2023, **861**, 160665.
32. K. Hu, P. Zhou, Y. Yang, T. Hall, G. Nie, Y. Yao, X. Duan and S. Wang, *ACS ES&T Engineering*, 2022, **2**, 110-120.
33. D. Ortiz, M. Munoz, J. Nieto-Sandoval, C. Romera-Castillo, Z. M. de Pedro and J. A. Casas, *Chemosphere*, 2022, **309**, 136809.
34. K. Bule Možar, M. Miloloža, V. Martinjak, F. Radovanović-Perić, A. Bafti, M. Ujević Bošnjak, M. Markić, T. Bolanča, M. Cvetnić, D. Kučić Grgić and Š. Ukić, *Journal*, 2024, **16**.
35. S. Ghatge, Y. Yang, Y. Ko, Y. Yoon, J.-H. Ahn, J. J. Kim and H.-G. Hur, *Journal of Hazardous Materials*, 2022, **423**, 127067.
36. C.-F. Chow, W.-L. Wong, K. Y.-F. Ho, C.-S. Chan and C.-B. Gong, *Chemistry – A European Journal*, 2016, **22**, 9513-9518.
37. V. S. Nguyen, Y. Chang, E. V. Phillips, J. A. DeWitt and C. Sievers, *ACS Sustainable Chemistry & Engineering*, 2023, **11**, 7617-7623.
38. Y. Liu and J. Wang, *Chemical Engineering Journal*, 2023, **466**, 143147.
39. J. P. Ribeiro, H. G. M. F. Gomes, L. Sarinho, C. C. Marques and M. I. Nunes, *Chemical Engineering and Processing - Process Intensification*, 2022, **181**, 109159.
40. X. Li, Z. Tian, K. Liang and Y. Wang, *Journal of Photochemistry and Photobiology A: Chemistry*, 2019, **379**, 79-87.
41. H. Lu, Z. Zhu, H. Zhang, J. Zhu, Y. Qiu, L. Zhu and S. Küppers, *ACS Applied Materials & Interfaces*, 2016, **8**, 25343-25352.
42. Y. Diao, Z. Yan, M. Guo and X. Wang, *Journal of Hazardous Materials*, 2018, **344**, 829-838.
43. E. G. Heckert, S. Seal and W. T. Self, *Environmental Science & Technology*, 2008, **42**, 5014-5019.
44. T. Montini, M. Melchionna, M. Monai and P. Fornasiero, *Chemical Reviews*, 2016, **116**, 5987-6041.
45. O. H. Laguna, M. A. Centeno, G. Arzamendi, L. M. Gandía, F. Romero-Sarria and J. A. Odriozola, *Catalysis Today*, 2010, **157**, 155-159.
46. A. Gogoi, M. Navgire, K. C. Sarma and P. Gogoi, *Chemical Engineering Journal*, 2017, **311**, 153-162.
47. L. Xu and J. Wang, *Environmental Science & Technology*, 2012, **46**, 10145-10153.
48. O. H. Laguna, M. A. Centeno, M. Boutonnet and J. A. Odriozola, *Applied Catalysis B: Environmental*, 2011, **106**, 621-629.
49. H. Wang and G. Tsilomelekis, *Catalysis Science & Technology*, 2020, **10**, 4362-4372.
50. Y. Qi, Q. Zuo, Y. Mei, T. Yao and J. Wu, *ACS Applied Nano Materials*, 2020, **3**, 7152-7160.
51. X. Shen, Z. Cai, J. Hu and B. Sun, *ChemistrySelect*, 2022, **7**, e202200804.
52. P. D. Muley, Y. Wang, J. Hu and D. Shekhawat, in *Catalysis: Volume 33*, eds. J. Spivey, Y.-F. Han and D. Shekhawat, The Royal Society of Chemistry, 2021, vol. 33, p. 0.
53. K. Faust, P. Denifl and M. Hapke, *ChemCatChem*, 2023, **15**, e202300310.
54. D. Mukherjee, B. G. Rao and B. M. Reddy, *Applied Catalysis B: Environmental*, 2016, **197**, 105-115.
55. H. Bao, X. Chen, J. Fang, Z. Jiang and W. Huang, *Catalysis Letters*, 2008, **125**, 160-167.
56. S. Loridant, *Catalysis Today*, 2021, **373**, 98-111.
57. , 1997, **15**, 533-559.
58. M. Qayoom, K. A. Shah, A. H. Pandit, A. Firdous and G. N. Dar, *Journal of Electroceramics*, 2020, **45**, 7-14.
59. H. Liu, Y. Wu, L. Liu, B. Chu, Z. Qin, G. Jin, Z. Tong, L. Dong and B. Li, *Applied Surface Science*, 2019, **498**, 143780.

60. A. Rahdar, M. Aliahmad, M. Samani, M. HeidariMajd and M. A. B. H. Susan, *Ceramics International*, 2019, **45**, 7950-7955.
61. T. Tsoncheva, C. Rosmini, M. Dimitrov, G. Issa, J. Henych, Z. Němečková, D. Kovacheva, N. Velinov, G. Atanasova and I. Spassova, *ACS Applied Materials & Interfaces*, 2021, **13**, 1838-1852.
62. K. I. Maslakov, Y. A. Teterin, A. J. Popel, A. Y. Teterin, K. E. Ivanov, S. N. Kalmykov, V. G. Petrov, P. K. Petrov and I. Farnan, *Applied Surface Science*, 2018, **448**, 154-162.
63. K. I. Maslakov, Y. A. Teterin, M. V. Ryzhkov, A. J. Popel, A. Y. Teterin, K. E. Ivanov, S. N. Kalmykov, V. G. Petrov, P. K. Petrov and I. Farnan, *Physical Chemistry Chemical Physics*, 2018, **20**, 16167-16175.
64. E. Bêche, P. Charvin, D. Perarnau, S. Abanades and G. Flamant, *Surface and Interface Analysis*, 2008, **40**, 264-267.
65. S. Soni, V. Srivats, S. Kumar, B. Dalela, M. Mishra, R. Singh, G. Gupta, D. P. Alvi and S. Dalela, *Journal of Materials Science: Materials in Electronics*, 2018, **29**.
66. T. Hasegawa, S. M. F. Shahed, Y. Sainoo, A. Beniya, N. Isomura, Y. Watanabe and T. Komeda, *The Journal of Chemical Physics*, 2014, **140**, 044711.
67. T. Yamashita and P. Hayes, *Applied Surface Science*, 2008, **254**, 2441-2449.
68. P. S. Bagus, C. J. Nelin, C. R. Brundle, B. V. Crist, N. Lahiri and K. M. Rosso, *Physical Chemistry Chemical Physics*, 2022, **24**, 4562-4575.
69. J.-C. Dupin, D. Gonbeau, P. Vinatier and A. Levasseur, *Physical Chemistry Chemical Physics*, 2000, **2**, 1319-1324.
70. Y. Xu, H. Zhang, D. Gong, Y. Chen, S. Xu and P. Qiu, *Journal of Materials Science*, 2022, **57**, 19716-19729.
71. R. Si and M. Flytzani-Stephanopoulos, *Angewandte Chemie International Edition*, 2008, **47**, 2884-2887.
72. X. Wei, X. Rang, W. Zhu, M. Xiang, Y. Deng, F. Jiang, R. Mao, Z. Zhang, X. Kong and F. Wang, *Chemical Physics*, 2021, **542**, 111079.
73. S. Liu, X. Liao, Q. Zhang, Y. Zhang, H. Wang and Y. Zhao, *Journal*, 2022, **12**.
74. S. N. Matussin, F. Khan, M. H. Harunsani, Y.-M. Kim and M. M. Khan, *ACS Omega*, 2023, **8**, 11868-11879.
75. I. Ali, E. A. Neskoromnaya, A. V. Melezhik, A. V. Babkin, B. A. Kulnitskiy, A. E. Burakov, I. V. Burakova, A. G. Tkachev, A. S. A. Almalki and A. Alsubaie, *Journal of Porous Materials*, 2022, **29**, 545-557.
76. P. Thomas, P. Sreekanth and K. E. Abraham, *Journal of Applied Physics*, 2015, **117**, 053103.
77. F. Scé, I. Cano, C. Martin, G. Beobide, Ó. Castillo and I. de Pedro, *New Journal of Chemistry*, 2019, **43**, 3476-3485.
78. É. Casey, R. Breen, G. Pareras, A. Rimola, J. D. Holmes and G. Collins, *RSC Sustainability*, 2024, **2**, 1040-1051.
79. H. Li, C. Zhang, C. Pang, X. Li and X. Gao, *Frontiers in Chemistry*, 2020, **8**.
80. E. Selvam, Y. Luo, M. Ierapetritou, R. F. Lobo and D. G. Vlachos, *Catalysis Today*, 2023, **418**, 114124.
81. D. Lefort, J. Fossey, M. Gruselle, J.-Y. Nedelec and J. Sorba, *Tetrahedron*, 1985, **41**, 4237-4252.
82. M. D. Argyle and C. H. Bartholomew, *Journal*, 2015, **5**, 145-269.
83. Y. Wang, X. Shen and F. Chen, *Journal of Molecular Catalysis A: Chemical*, 2014, **381**, 38-45.
84. T. J. Smak, P. de Peinder, J. C. Van der Waal, R. Altink, I. Vollmer and B. M. Weckhuysen, *ChemSusChem*, 2024, **17**, e202301198.
85. A. Pifer and A. Sen, *Angewandte Chemie International Edition*, 1998, **37**, 3306-3308.
86. R. Zafar, S. Y. Park and C. G. Kim, *Environmental Engineering Research*, 2022, **27**, 210028-210020.
87. C.-C. Kuan, S.-Y. Chang and S. L. M. Schroeder, *Industrial & Engineering Chemistry Research*, 2015, **54**, 8122-8129.

88. Y. Chen, C. J. Miller and T. D. Waite, *Environmental Science & Technology*, 2021, **55**, 14414-14425.
89. N. Zhang, J. Chen, Z. Fang and E. P. Tsang, *Chemical Engineering Journal*, 2019, **369**, 588-599.
90. N. Zhang, E. P. Tsang, J. Chen, Z. Fang and D. Zhao, *Journal of Colloid and Interface Science*, 2020, **558**, 163-172.
91. M. M. Bello, A. A. Abdul Raman and A. Asghar, *Process Safety and Environmental Protection*, 2019, **126**, 119-140.
92. M. Munoz, Z. M. de Pedro, J. A. Casas and J. J. Rodriguez, *Applied Catalysis B: Environmental*, 2015, **176-177**, 249-265.
93. E. M. Bevilacqua, E. S. English and J. S. Gall, *Journal of Applied Polymer Science*, 1964, **8**, 1691-1698.
94. A. D. Bokare and W. Choi, *Journal of Hazardous Materials*, 2014, **275**, 121-135.
95. S.-S. Lin and M. D. Gurol, *Environmental Science & Technology*, 1998, **32**, 1417-1423.
96. P. Ji, L. Wang, F. Chen and J. Zhang, *ChemCatChem*, 2010, **2**, 1552-1554.